

Modeling and Analysis of a Slurry Reactor System for Heterogeneous Olefin Polymerization: The Effects of Hydrogen Concentration and Initial Catalyst Size

KYOUNG-SU HA, KEE-YOUN YOO, HYUN-KU RHEE

School of Chemical Engineering and Institute of Chemical Processes, Seoul National University, Seoul, 151-742, Korea

Received 22 October 1999; accepted 20 June 2000

ABSTRACT: This article deals with the development of a model for the polymerization process using a Ziegler-Natta catalyst in a slurry reactor system. Employed here is the hierarchical model describing the entire reactor system that is subcategorized by the gas bubble phase, the continuous gas phase, the liquid phase, the solid polymer particle, and the surface of catalyst where chemical reaction occurs. The concept of the multigrain model (MGM) is introduced to describe the growth of polymer particle from the original catalyst particle. We also adopt the concept of multiple active sites to elucidate the broad molecular weight distribution (MWD). The major concern here is the effects of the hydrogen concentration and the size of the initial catalyst on the performance of the polymerization reactor. It is demonstrated that the hydrogen gas can be used for the purpose of controlling not only the molecular weight but the molecular weight distribution (MWD) of the polymer. In addition, the relationship between the molecular weight and the concentration of hydrogen gas is investigated. The size of the initial catalyst is found to exercise a significant influence on the morphology of the resultant polymer particle. © 2001 John Wiley & Sons, Inc. *J Appl Polym Sci* 79: 2480–2493, 2001

Key words: polyethylene; Ziegler-Natta; molecular weight; multigrain model; slurry reactor; hydrogen

INTRODUCTION

In the heterogeneous Ziegler-Natta polymerization process, the polymer product usually obtains a broad molecular weight distribution (MWD), the reason for which has not been well understood. According to the previous reports, the heterogeneous nature of the catalyst,^{1,2} as well as the mass transfer resistance,^{3–5} should be considered in order to elucidate the cause for the broad MWD.

On the basis of transmission electron microscope experiments Kakugo et al.⁶ reported that

an olefin polymer particle produced over the heterogeneous Ziegler-Natta catalyst is composed of a set of microparticles, each of which contains a catalyst fragment at the center. In view of the above feature of growing polymer particles various mathematical models have been developed for the olefin polymerization such as multigrain model (MGM),^{7–9} continuous flow (polymeric flow) model,^{10,11} etc. Among them, the MGM is known to describe the growing polymer particles very closely to the observations by scanning electron microscope.

In their simulation study for the growing polymer particles, Laurence and Chiovetta¹² presented the numerical solution for mass and energy balance equations considering the breakage of catalyst particle in the beginning of reaction.

Correspondence to: H.-K. Rhee.

Journal of Applied Polymer Science, Vol. 79, 2480–2493 (2001)
© 2001 John Wiley & Sons, Inc.

Table I Elementary Chemical Reactions Occurring in Olefin Polymerization

Description		Reaction
Activation by aluminum alkyl (A)	Activation	$C_p(j) + A \xrightleftharpoons{K_a(j)} C^*(j)$ (1)
Initiation of M by normal active center	Initiation	$C^*(j) + M \xrightarrow{k_i(j)} R_1(j)$ (2)
Propagation of chain with M	Propagation	$R_n(j) + M \xrightarrow{k_p(j)} R_{n+1}(j)$ (3)
Chain transfer to hydrogen (H_2)	Chain transfer	$R_n(j) + H_2 \xrightarrow{k_m(j)} C^*(j) + P_n(j)$ (4)

Also, Floyd¹³ obtained an analytical solution for the profiles of monomer concentration in the polymer particle and in the microparticle using the quasi-steady state hypothesis (QSSH) and the numerical solution without using the QSSH. According to their results, the broad MWD cannot be fully explained by mass transfer resistance in the polymer particle alone, but they suggested that the concept of multiple active sites having different reaction characteristics might account for the broad MWD.

Hutchinson et al.¹⁴ extended Floyd's model to apply it to the copolymerization system. These authors radially divided a polymer particle into shells to compute the mass balance equations numerically, then probed the gradient of monomer concentration and the voidage in the particle, and examined the effects of irregular distribution of active sites in the particle. Also, Xie et al.¹⁵ investigated the influence of the active site multiplicity on the MWD under various reaction conditions.

In this study we develop a multigrain model with two different kinds of active sites on the catalyst surface to analyze the effects of mass transfer resistance and active site heterogeneity on the polymer property as well as on the productivity. To establish a reactor-scale model we introduce the hierarchical modeling mentioned by Ray¹⁶ and rearrange it into a three-level hierarchical model. The Polymerization Reaction Mechanism section is concerned with the microscale phenomena as mentioned by Ray, whereas the Material Balances in Polymer Particle section deals with the phenomena of the polymer particle scale such as the growth of polymer particle and mass transport inside and near the particle surface. The Reactor Modeling section describes the phenomena on the reactor scale, and thus treats the mass transfer of monomer from hydrocarbon medium to a growing polymer particle and the variations of monomer concentrations in the liquid phase as well as in the continuous gas phase.

Above all, the model developed here is validated by comparing the simulation results with the reported experimental data and the information from the industries given in Tables III and IV. This is then followed by the analysis of the effects of hydrogen concentration and initial catalyst size on the polymer properties and the productivity. In addition, the relationship between the number-average molecular weight and hydrogen concentration is discussed.

OLEFIN POLYMERIZATION KINETICS

Polymerization Reaction Mechanism

The cocatalyst A is adsorbed on the potential active site of type j , $C_p(j)$, which exists on the catalyst surface, and then the potential active site becomes the active site of type j , $C^*(j)$. Reaction (2) in Table I shows that $C^*(j)$ will react with monomer M to yield a live polymer chain with unit length $R_1(j)$. The subscript in the live polymer chain denotes the number of monomer units. When an excess of cocatalyst is used, it is reasonable to assume that all the potential sites become vacant active sites. Thus, reaction (1) in Table I may not be considered.

In this study, the two-step mechanism is adopted because it is rather simple and the stereoregulation is not of our concern here. Following Natta,¹⁷ we assume that the first step is rate determining. Thus, we can simply express the propagation step of olefin polymerization as reaction (3) in Table I, where $R_n(j)$ represents a live polymer chain that is attached to the active site of type j and has the n repeating units, and $k_p(j)$ is the rate constant for the propagation reaction.

In olefin polymerization with a Ziegler-Natta catalyst, the chain transfer reaction can proceed with the participation of monomer, cocatalyst, and hydrogen, respectively, or via the hydride

shift. The contribution of chain transfer to organoaluminium cocatalyst (OAC) in the case of $\text{TiCl}_4/\text{MgCl}_2$ is insignificant because the type and concentration of OAC has no influence on the molecular weight of polyethylene.¹⁸ In the case of the chain transfer to hydrogen, the rate constant k_{FH} of the $\text{TiCl}_4/\text{MgCl}_2$ catalyst system (first-order chain transfer with respect to hydrogen concentration) is much higher than that of the TiCl_3 catalyst system (0.5th order with respect to hydrogen concentration). Because the chain transfer to hydrogen especially in the $\text{TiCl}_4/\text{MgCl}_2$ catalyst system proceeds much faster than any other chain transfer such as the chain transfer to the cocatalyst, monomer, etc., the concentration of the hydrogen would significantly influence the molecular weight of the polymer. In this study, therefore, we consider only the role of hydrogen in the chain transfer reaction, as shown by reaction (4) in Table I.

For the reaction mechanism of Table I, one can derive the rate of formation for individual species. For $R_1(j)$, the rate of formation is expressed as

$$r(R_1(j)) = k_I(j)C^*(j)M - \{k_p(j)M + k_{FH}(j)H_2\}R_1(j) \quad (5)$$

where M and H_2 are the concentrations of monomer and hydrogen, respectively, around the active site. The concentration of unoccupied active site is given by

$$C^*(j) = C_0^*(j) - \mu_0^L(j) \quad (6)$$

where $\mu_0^L(j)$ represents the total concentration of the live polymer. For live polymer chains with $n \geq 2$, we obtain

$$r(R_n(j)) = k_p(j)R_{n-1}(j)M - \{k_p(j)M + k_{FH}(j)H_2\}R_n(j) \quad (7)$$

$$r(P_n(j)) = k_{FH}(j)H_2R_n(j) \quad (8)$$

Let us now consider the moments of live and dead polymer chains defined as

$$\mu_k^L(j) = \sum_{n=1}^{\infty} n^k R_n(j) \quad \text{and} \quad \mu_k^D(j) = \sum_{n=1}^{\infty} n^k P_n(j), \quad k = 0, 1, 2 \quad (9)$$

where the subscript k denotes the order of moments. The rate expressions for these moments can be derived as follows:

$$r(\mu_0^L(j)) = k_I(j)C^*(j)M - k_{FH}(j)H_2\mu_0^L(j) \quad (10)$$

$$r(\mu_1^L(j)) = k_I(j)C^*(j)M + k_p(j)M\mu_0^L(j) - k_{FH}(j)H_2\mu_1^L(j) \quad (11)$$

$$r(\mu_2^L(j)) = k_I(j)C^*(j)M + k_p(j)M\mu_0^L(j) + 2k_p(j)M\mu_1^L(j) - k_{FH}(j)H_2\mu_2^L(j) \quad (12)$$

$$r(\mu_0^D(j)) = k_{FH}(j)H_2\mu_0^L(j) \quad (13)$$

$$r(\mu_1^D(j)) = k_{FH}(j)H_2\mu_1^L(j) \quad (14)$$

$$r(\mu_2^D(j)) = k_{FH}(j)H_2\mu_2^L(j) \quad (15)$$

Whenever necessary, $\mu_k(j)$ without superscript L or D will be used to represent the k th moment of live and dead polymer concentrations on the active site of type j , and μ_k to represent the k th moment of live and dead polymer concentrations from all the active sites. The number-average molecular weight M_n , the weight-average molecular weight M_w , and the polydispersity PD are defined as follows:

$$M_n = \frac{\mu_1}{\mu_0} \times \text{MW}, \quad M_w = \frac{\mu_2}{\mu_1} \times \text{MW} \quad \text{and} \quad PD = \frac{M_w}{M_n} \quad (16)$$

where MW is the molecular weight of monomer.

Material Balances in Polymer Particle

The multigrain model is schematically shown in Figure 1. Let us consider the time scale for the mass transport to reach a quasi-steady state. The time constant τ_s for the monomer concentration to reach a quasi-steady state in the microparticle is approximately given by

$$\tau_s = \frac{r_s^2}{D_s} \quad (25)$$

where r_s and D_s denote the radius of a microparticle in a polymer particle and the diffusion coefficient of monomer in the microparticle, respec-

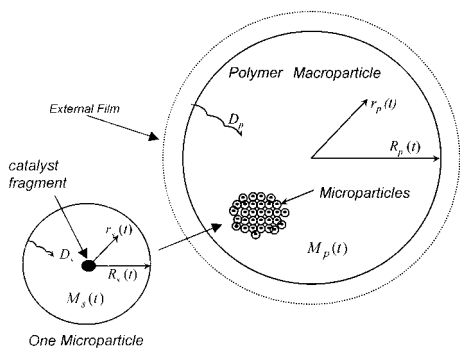


Figure 1 Schematic diagram of the multigrain model.

tively.¹³ If we assume that the variation with time of the concentration profile in microparticle is negligible and apply the quasi-steady state hypothesis (QSSH), integration of material balance eq. (21) in Table II gives

$$M_{\text{crys}} = \eta^* M_p - \frac{r_{\text{crys}}^2}{3D_s} \text{Rate}_s \left(1 - \frac{1}{\phi}\right) \quad (26)$$

where η^* denotes the partition coefficient, and the microparticle growth factor ϕ is defined as

$$\phi = \frac{R_s}{r_{\text{crys}}} \quad (27)$$

According to Hutchinson et al.,¹⁴ the partition coefficient may be determined by the equation

$$\eta^* = 1.0 - \nu_{\text{pol}} \quad (28)$$

where ν_{pol} is the volume fraction of polymer in the swollen amorphous polymer phase. The partition coefficient η^* is empirically related to the system temperature by Hutchinson et al.¹⁴

Although eq. (26) indicates that the concentration gradient across the polymer layer increases as the microparticle grows in size, the degree of diffusion resistance in the microparticle rapidly approaches an asymptotic value and is practically constant for $\phi > 10$.¹⁹ The volumetric rate of consumption in the macroparticle denoted by Rate_p may be expressed as

$$\text{Rate}_p = \text{Rate}_s \times \left(\frac{1 - \epsilon}{\phi^3}\right) \quad (29)$$

where Rate_s is the rate of polymerization per unit mass of catalyst in the macroparticle at a certain radial position, and ϵ denotes the local microparticle void fraction.

REACTOR MODELING

Description of Semibatch Slurry Reactor

In this study we consider the gas–liquid and liquid–solid interphase mass transfer resistances,

Table II Mass Balance Equations of the Multigrain Model for the Solid Phase

$$\square \text{ Macroparticle } (0 \leq r_p \leq R_p) \quad \frac{\partial M_p}{\partial t} = \frac{1}{r_p^2} \frac{\partial}{\partial r_p} \left(D_p r_p^2 \frac{\partial M_p}{\partial r_p} \right) - \text{Rate}_p \quad (17)$$

$$\text{B.C.} \quad r_p = 0: \quad \frac{\partial M_p}{\partial r_p} = 0 \quad (18)$$

$$r_p = R_p: \quad D_p \frac{\partial M_p}{\partial r_p} = k_s (M_l - M_{p,s}) \quad (19)$$

$$\text{I.C.} \quad t = 0: \quad M_p = M_0 \quad \text{at} \quad R_p = R_{\text{cat}} \quad (20)$$

$$\square \text{ Microparticle } (r_{\text{crys}} \leq r_s \leq R_s) \quad \frac{\partial M_s}{\partial t} = \frac{1}{r_s^2} \frac{\partial}{\partial r_s} \left(D_s r_s^2 \frac{\partial M_s}{\partial r_s} \right) \quad (21)$$

$$\text{B.C.} \quad r_s = R_s: \quad M_s = \eta^* M_p \quad (22)$$

$$r_s = r_{\text{crys}}: \quad 4\pi r_{\text{crys}}^2 D_s \frac{\partial M_s}{\partial r_s} = \frac{4\pi}{3} r_{\text{crys}}^3 \text{Rate}_s \quad (23)$$

$$\text{I.C.} \quad t = 0: \quad M_{s,i} = M_{0,i} \quad \text{at} \quad R_s = r_{\text{crys}} \quad (24)$$

The phases considered in the slurry reactor are the gas phase, the liquid phase, the gas bubble phase, and the solid phase.

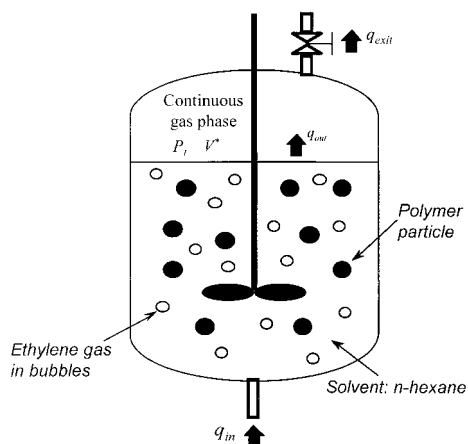


Figure 2 Schematic diagram of the semibatch slurry olefin polymerization reactor.

which could play important roles during polymerization with highly active catalysts. The importance of these resistances have been emphasized by Floyd et al.¹⁹ The semibatch reactor is shown schematically in Figure 2.

Initially there is a volume of V_l of slurry, which contains liquid solvent (*n*-hexane) and N_0 solid catalyst particles, all of which are assumed to be spherical and have the same radius R_{cat} . The vapor-filled space (continuous gas phase) of volume V^* above the liquid slurry is occupied by gas phase ethylene at 1 atm. At time $t = 0$, pure gas-phase ethylene is bubbled into the reactor at a rate of q_{in} , and hydrogen gas is also bubbled into the reactor to control the molecular weight. We assume perfect mixing of the liquid phase and the continuous gas phase, respectively, in the reactor.

Monomer dissolves partially in the solvent, and diffuses toward the catalyst particles through the liquid *n*-hexane. The rate at which monomer transfers from the well-dispersed gas bubbles to the liquid solvent will be controlled by the overall

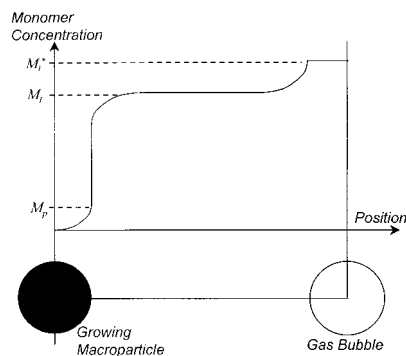


Figure 3 Monomer concentration profile with location at an arbitrary time.

gas-liquid mass transfer rate. If an excess of monomer is bubbled in, the excess portion will go to the vapor space (continuous gas phase V^*) above the slurry. Bubbled monomer moves from the continuous liquid phase to the solid particles. Here, again, the rate at which monomer transfers from the continuous liquid phase to the solid phase particles will also be controlled by the liquid–solid mass transfer rate. Monomer diffuses radially into the porous polymer particle. Under these circumstances the distribution of monomer may be depicted, as shown in Figure 3.

In this process, polymerization occurs at each active site of catalyst surface. The polymer particle grows radially outwards as produced polymer chains accumulate and mingle among themselves. Immediately after the beginning of polymerization, the original catalyst breaks into catalyst fragments (also called catalyst crystallites), which are assumed to be all equal in size and are dispersed in the continuum of polymer matrix. Polymer chains grow surrounding a catalyst fragment, which results in a spherical polymer subparticle called a microparticle. These microparticles from one original catalyst particle form one

Table III Molecular Weights and Polydispersities of High Density Polyethylene Obtained with Some Traditional, Supported Ziegler-Natta Catalytic Systems

Catalytic System	Temperature (°C)	MW Control with H ₂	$M_n \times 10^{-3}$ (g/mol)	$M_w \times 10^{-3}$ (g/mol)	PD	Ref.
TiCl ₄ + Mg(OC ₂ H ₅) ₂	70	Yes	17	120	7.0	30
α -TiCl ₃ · 0.3AlCl ₃	70	No	340	2700	8	39
TiCl ₄	70	No	180	2160	12.0	39
TiCl ₄ on activated carbon	70	No	300	5400	18.0	39
TiCl ₄ on silica-alumina	70	No	300	2990	10.0	39
TiCl ₄ on MgO	70	No	1000	2920	2.9	39

Table IV Catalytic Activities Reported by Representative Commercial Plants²³

Commercial Industries	Reactor Type	Temperature (°C)	Pressure (atm)	Catalytic System	Activity (g/g cat)	MW Control
Phillips	Loop	85–100	30–35	Supported Cr catalyst	3,000–10,000	Temperature
Solvay	Loop	80	30	Mg-supported ZN-catalyst	11,000	H ₂
Hoechst, Montedison, Dow, Mitsubishi	CSTR	80–90	1.8–35	Mg-supported ZN catalyst	3000	H ₂

macroparticle. This model is well known as the multigrain model (MGM).

In the early stage of operation the monomer bubbled in increases its concentration in the liquid phase. Slowly, an excess of monomer accumulates (at a rate of q_{out}) at the top of the reactor, and thus the pressure P_t builds up. The rate of release of monomer from the reactor, q_{exit} , is set in such a way that the pressure P_t goes up to a value of P_{max} and is then maintained at this value. For simplicity, we assume that the reactor is isothermal.

Mass Balance Equations

The reactor system is composed of four parts; i.e., solid phase, liquid phase, gas bubble phase, and continuous gas phase. In each phase we set up appropriate equations on the basis of mass balance. To calculate the mass transfer coefficients for the gas–liquid interface and the liquid–solid interface several correlation equations were used.²⁰

Solid phase (Growing Polymer Particle)

The equations for solid phase are listed in Table II. The solid phase is the term describing the macroparticles containing microparticles. All the growing macroparticles and microparticles are assumed to be identical, respectively, at any time

Table V Reference Reaction Conditions for the Semibatch Slurry Reactor

Temperature	80°C
Maximum pressure	8 atm
$k_p(1)$	10.0 m ³ /mol · s
$k_p(2)$	1.0 m ³ /mol · s
Concentration of hydrogen	7.5 mol/m ³
Initial radius of catalyst particle	10 μ

t and, thus, only one set of equations are necessary for macroparticles as well as for microparticles.

Liquid Phase

In the perfectly mixed liquid phase where *n*-hexane is the continuous phase, the mass balance for monomer yields the equation

$$V_l \frac{dM_l}{dt} = k_{gl}a_{gl}(V_g + V_l)(M_l^* - M_l) - k_{ls}a_{ls}(V_l + V_s)(M_l - M_{p,s}) \quad (30)$$

where M_l represents the monomer concentration in the liquid phase, M_l^* the equilibrium concentration at the gas–liquid interface at a given pressure and temperature, and $M_{p,s}$ the concentration at the surface of the growing polymer particle. The equilibrium concentration M_l^* is calculated by the Peng-Robinson equation and UNIQUAC method.^{21,22} The first term on the right-hand side of eq. (30) represents the mass transfer rate from the gas bubble phase to the liquid phase, and the second is the mass transfer rate from the liquid phase to the solid phase; i.e., the growing polymer particle.

Gas Bubble Phase

The material balance equation for the gas bubble phase, which is well distributed in the liquid *n*-hexane, may be written as

Table VI Dimensions of the Semibatch Slurry Reactor

Reactor diameter	1.5 m
Reactor volume	20 m ³
Volume of continuous gas phase	4 m ³
Impeller diameter	0.5 m

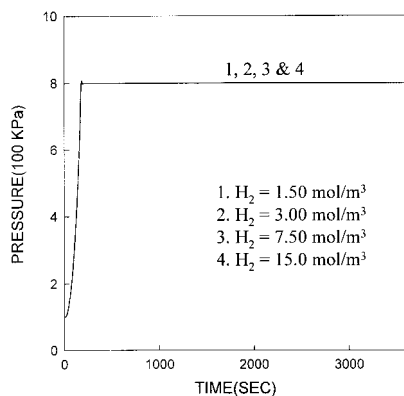


Figure 4 Time evolution of the total pressure under various hydrogen concentrations.

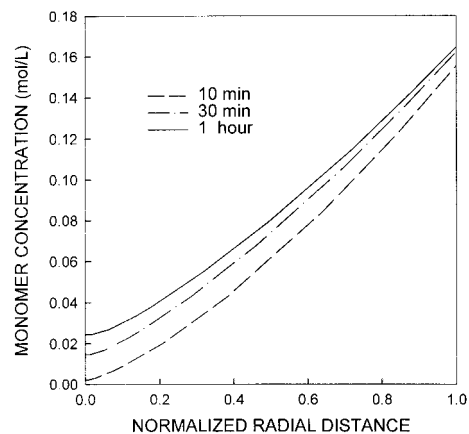
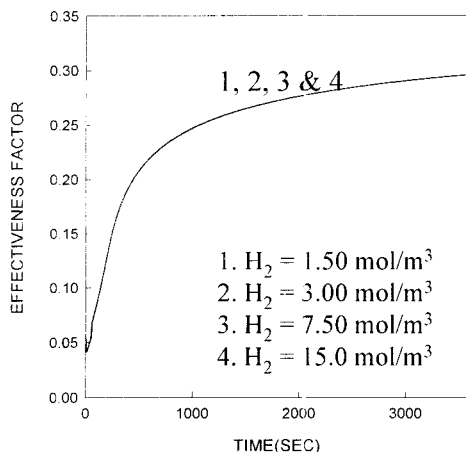
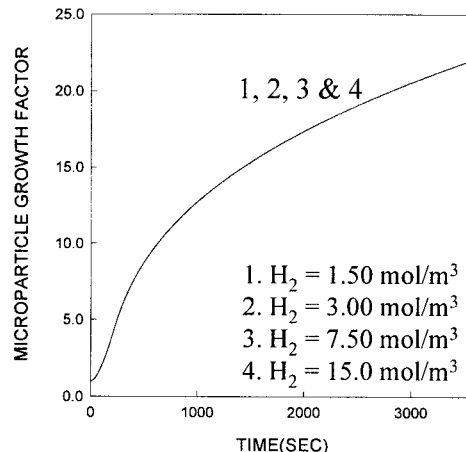


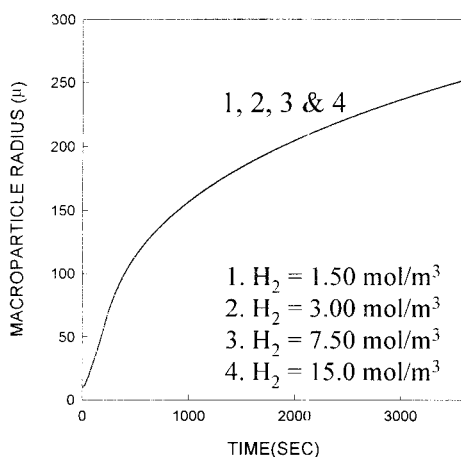
Figure 5 Development of intramacroparticle distribution of monomer under the reference reaction conditions.



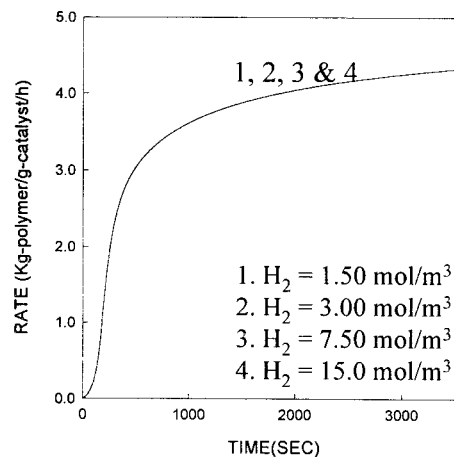
(a) Effectiveness factor



(b) Microparticle growth factor



(c) Size of macroparticle



(d) Overall reaction rate

Figure 6 Time histories of effectiveness factor, microparticle growth factor, size of macroparticle, and overall reaction rate under various hydrogen concentrations: (a) effectiveness factor; (b) microparticle growth factor; (c) size of macroparticle; (d) overall reaction rate.

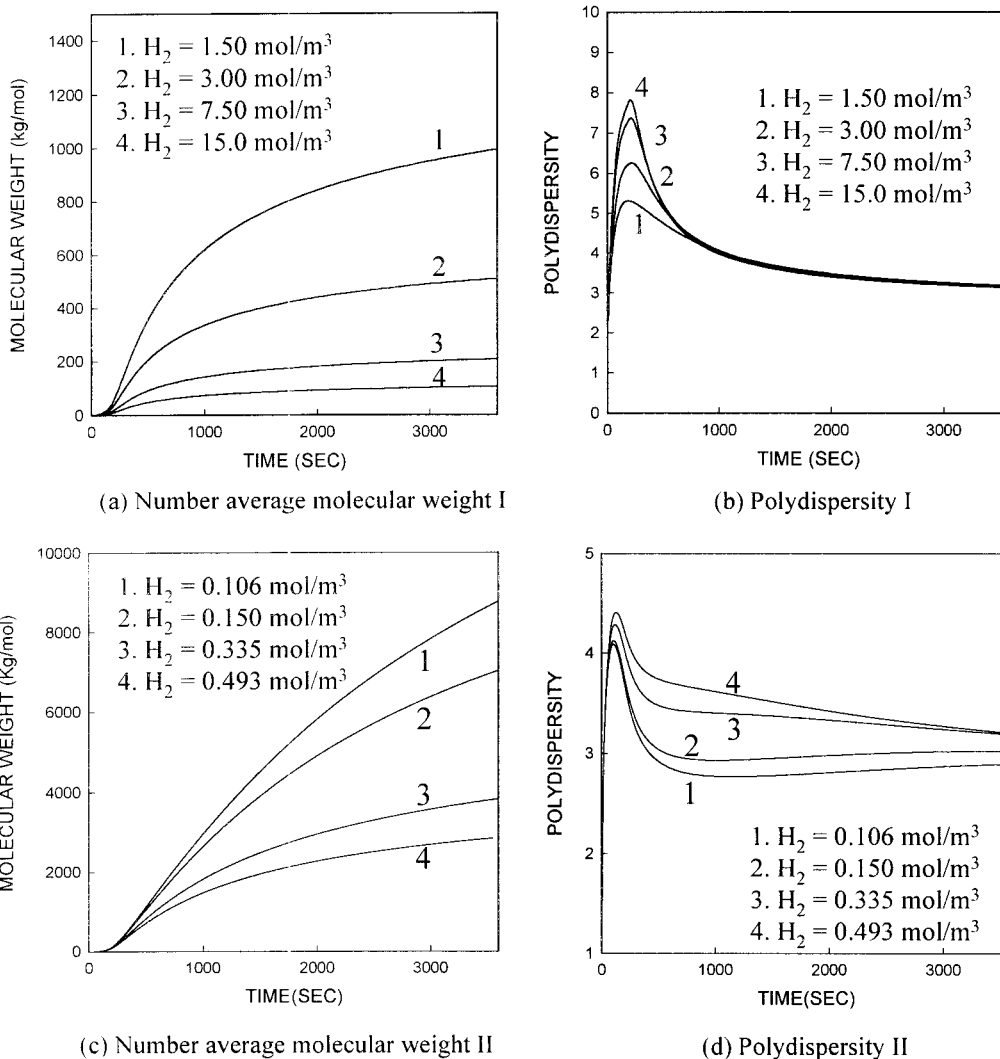


Figure 7 Time histories of number-average molecular weight and polydispersity under various hydrogen concentrations: (a) number-average molecular weight I; (b) polydispersity I; (c) number-average molecular weight II; (d) polydispersity II.

$$q_{\text{out}} = q_{\text{in}} - k_{gl}\alpha_{gl}(V_g + V_l)(M_l^* - M_l) \quad (31)$$

where the left-hand side is the rate of accumulation in the continuous gas phase above the liquid phase. On the right-hand side the first term q_{in} denotes the bubbling rate from the reactor bottom, and the second is the rate from the gas bubble to the liquid phase. If the second term exceeds the first, the former will be set equal to the second term, so the left-hand side will be equal to zero.

Continuous Gas Phase

Due to the inflow of monomer gas bubbles the pressure in the continuous gas phase builds up to

the maximum value P_{max} with time, which is governed by the following equation:

$$\frac{dP_t}{dt} = \left(\frac{q_{\text{out}} - q_{\text{exit}}}{V^*} \right) RT \quad (32)$$

where we have assumed ideal gas behavior and R denotes the universal gas constant.

SIMULATION RESULTS AND DISCUSSION

In this study a single slurry reactor for ethylene polymerization is modeled and simulated with *n*-hexane as hydrocarbon diluent. We assume

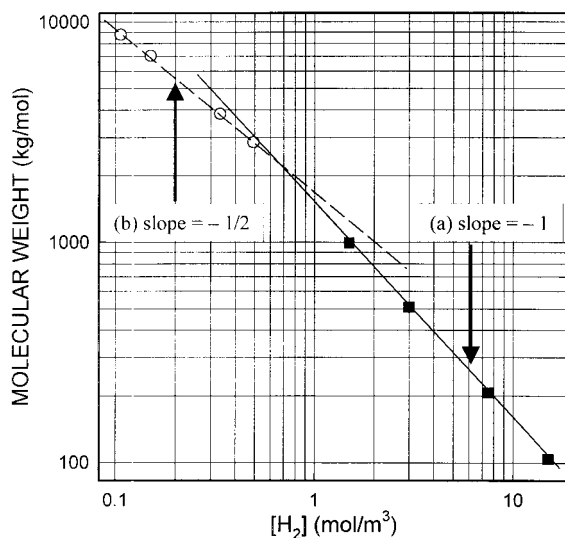


Figure 8 Relationship between the hydrogen concentration and number-average molecular weight: (a) $[H_2] = 1.50, 3.00, 7.50,$ and 15.0 mol/m^3 , and (b) $[H_2] = 0.106, 0.150, 0.335,$ and 0.493 mol/m^3 .

that two different kinds of active sites are present in catalyst. The rate constant for the lower activity is 10 times as low as that for the higher, where the latter value is chosen on the basis of the reported data.^{23,24}

We consider that a valve is installed on the top of the reactor body to regulate the total pressure. The equation of state mentioned above is used to calculate the gas-liquid equilibrium concentrations under given temperature and pressure varying with monomer influx. The states of the system are computed from the start-up to near the steady state. Here, we are mainly concerned with the effects of the hydrogen concentration and the initial size of catalyst particle on the performance of Ziegler-Natta catalytic system in a slurry reactor.

For the purpose of making comparison, we have taken the data on Ziegler-Natta catalytic system from the literature. Molecular weights and polydispersities of high density polyethylene obtained with some traditional, supported Ziegler-Natta catalytic systems are tabulated in Table III. Polydispersity values ranging from around 3 to 18 in this table indicate that some catalysts can produce polymer products with very broad MWD. The activity data for industrial processes under different reaction conditions are also presented in Table IV. The reference reaction conditions and the reactor dimensions are given in Tables V and VI, respectively.

Effect of Hydrogen Concentration

Figure 4 shows the variation of the total pressure with the reaction time under four different hydrogen concentrations. The total pressure is found to increase rapidly from its initial value of 1 atm and reaches its maximum value of 8 atm within 200 s. It is clearly seen that the hydrogen concentration has negligible effect on the total pressure.

The time evolution of the intra-macroparticle monomer distribution is depicted in Figure 5. The concentration profiles are given at three different times under the reference reaction conditions, but almost the same profiles are obtained for three different hydrogen concentrations; i.e., 1.50, 3.00, and 15.0 mol/m^3 . The monomer concentration at the center increases slowly to reach its steady-state value at about 1 h. At this stage the monomer concentration at the center is approximately equal to one-sixth of the concentration at the surface, which has increased slightly because the extended surface area leads to the enhancement of the mass transfer.

In Figure 6 we present the time histories of the effectiveness factor, the microparticle growth factor, the size of macroparticle, and the overall reaction rate. It is to be noticed that all the four factors are not influenced by the hydrogen concentration. Although the effectiveness factor remains low—approximately 0.3 on the average over the period of 1 h, the overall yield of polymer registers about 4 kg-polymer/g-catalyst for 1 h as may be seen from Figure 6(d), and this value is in good agreement with those from the commercial processes using the slurry reactor of CSTR type (cf. Table IV). In Figure 6(b) and (c), one can see that, regardless of the hydrogen concentration, the size of the microparticle increases to be 20 times larger than that of the initial catalyst and the macroparticle grows up to around 250 μ or higher after 1 h. In the earlier stage of operation, the growth rate increases very rapidly, and then tends to slow down because Rate_p decreases as polymer particles grow [cf. eq. (29)].

Figure 7 presents the variations of the number-average molecular weight and the polydispersity with the reaction time. In Figure 7(a) and (c), the molecular weight is found to increase steadily in contrast to the case of free radical polymerization mechanism, in which the molecular weight instantly jumps up to its steady-state value. It is to be particularly emphasized that the molecular weight is very sensitive to the hydrogen concentration. In Figure 7(a), an increase of hydrogen

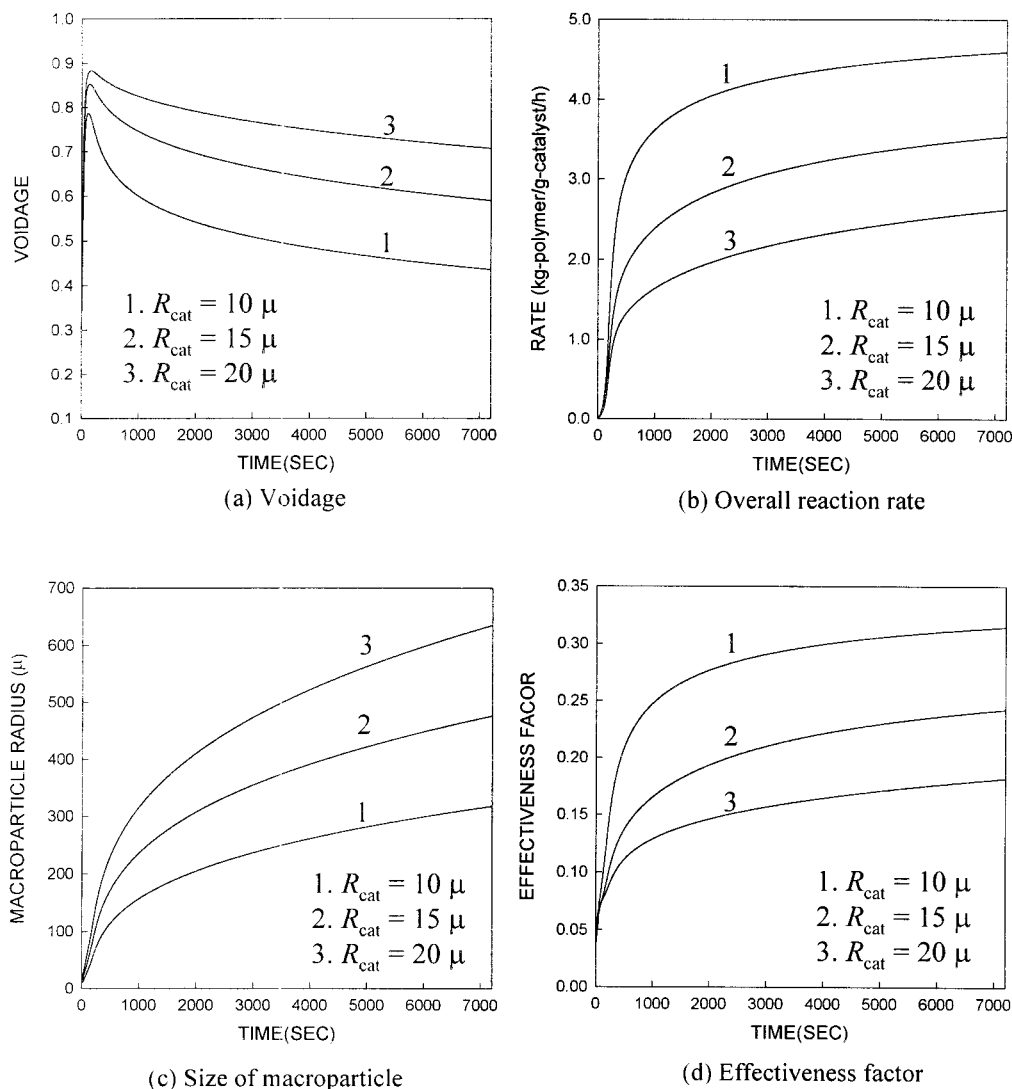


Figure 9 Time histories of voidage, overall reaction rate, size of macroparticle, and effectiveness factor for various initial catalyst sizes: (a) voidage; (b) overall reaction rate; (c) size of macroparticle; (d) effectiveness factor.

concentration from 1.5 mol/m^3 to 3.0 mol/m^3 gives rise to a decrease in the number-average molecular weight by 50%. It is noticed, however, from Figures 6(d) and 7(a) that hydrogen acts as a simple transfer agent because it reduces the molecular weight without affecting the rate of polymerization.²⁵

According to Natta,¹⁷ the rate of propagation is governed only by the nature of monomer entering into a polymer chain, and is independent of the nature of the last unit of the chain end bound to the titanium ion. Taking into account this feature and the chain transfer process, Grievson²⁶ suggested that the number-average molecular weight

is inversely proportional to the hydrogen concentration if only the chain transfer to hydrogen is considered; i.e.,

$$M_n \propto 1/[H_2] \quad (33)$$

In Figure 8(a), it is clearly observed that eq. (33) is valid when the hydrogen concentration is higher than 1.5 mol/m^3 . Similar results were also reported by different authors²⁷⁻³⁰ in regard to the homogeneous Ziegler-Natta catalytic system. On the other hand, one can see in Figure 8(b) that the number-average molecular weight is inversely

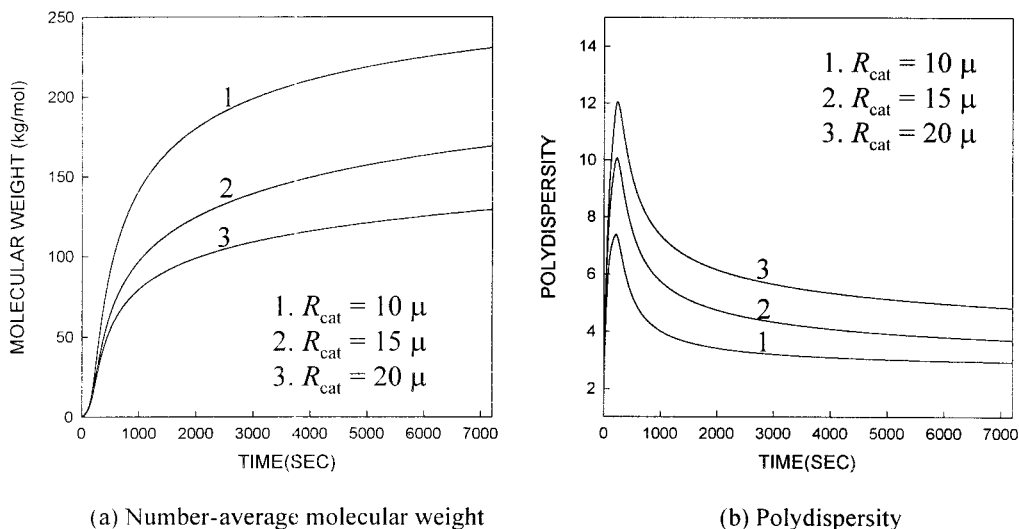


Figure 10 Time histories of number-average molecular weight and polydispersity for various initial catalyst sizes: (a) number-average molecular weight; (b) polydispersity.

proportional to $[H_2]^{1/2}$ if the hydrogen concentration is lower than 0.5 mol/m^3 .¹⁸ This is an interesting observation because the order of the chain transfer reaction is not 1/2 but 1 with respect to the hydrogen concentration, and the number-average molecular weight is roughly proportional to the rate of propagation over the rate of chain transfer in free radical polymerization.³¹ According to the results of the present study, however, the number-average molecular weight may be related to the hydrogen concentration as follows:

$$M_n \propto 1/[H_2] \quad (34)$$

in which n changes from 1/2 to 1 as the hydrogen concentration increases.

On the other hand, it is to be pointed out that the present model does not take into account the termination by hydride transfer, and transfers to monomer and cocatalyst. Inclusion of such reactions may change the relationship between the number-average molecular weight and the hydrogen concentration.¹⁸ With respect to the Grievson's relation, Reich and Schindler³² suggested that the hydrogen gas could affect the rate of polymerization, so the relation may be used only when the hydrogen gas does not affect the rate of polymerization.

In Figure 7(b) and (d), the polydispersity rapidly increases to the peak value, and immediately reduced to its steady state value in about 10 min. Some authors³³⁻³⁵ claimed that for polyethylene

obtained with traditional Ziegler-Natta catalytic systems, the polydispersity is independent of the hydrogen concentration, which is well supported by Figure 7(b). According to the experimental results of Yuan et al.,³⁶ however, polypropylene prepared with $TiCl_3 \cdot 1/3AlCl_3$ (Stauffer type AA)- $Al(C_2H_5)_2Cl$ showed slightly higher polydispersity with hydrogen than without hydrogen. Pegoraro³⁷ reported the same conclusion for propylene polymerization. More recently, Chien and Wang³⁸ also pointed out that polydispersity increased in the presence of hydrogen gas in ethylene polymerization with homogeneous Ziegler-Natta catalyst, and this is in accordance with Figure 7(d). Consequently, one may conclude that in the olefin polymerization the polydispersity increases as the hydrogen concentration goes up, but when the hydrogen concentration is larger than a critical value, which is about 0.3 mol/m^3 in this system, the steady-state value of polydispersity is independent of the hydrogen concentration.

Effect of Initial Catalyst Size

Figure 9 shows the time histories of the voidage, the overall reaction rate, the size of macroparticle, and the effectiveness factor for three different initial catalyst sizes. It is immediately evident that the effect of initial catalyst size is rather significant on all the four factors.

If a relatively large catalyst of radius greater than 15μ is used, the voidage of the resultant

polymer is found to be very high [cf. Fig. 9(a)]. Under this condition almost all the polymerization occurs near the surface, and the rapidly growing microparticles near the surface may be packed rather loosely. Therefore, the voidage near the outer shell of macroparticle becomes very high, and the voidage of the entire particle approaches the value of 0.7. On the contrary to the circumstances near the surface, the rate of polymerization near the center of the polymer particle would be very low. High voidage is not favorable from the viewpoint of productivity, because the yield will fall, as may be observed in Figure 9(b). It is, therefore, required to select a proper size of catalyst for the successful operation of a slurry reactor.

On the other hand, the size of resultant polymer particle increases markedly as the initial catalyst size increases, as shown in Figure 9(c). It is then obvious that, as the initial catalyst size increases, the diffusional resistance becomes large and the effectiveness factor falls significantly as shown in Figure 9(d). For the catalyst of 20 μ , the effectiveness factor becomes as low as around 0.16. In contrast to the productivity of 4.7 kg-polymer/g-cat./h for the reference catalyst of size 10 μ , the productivities for catalysts of 15 and 20 μ are found to be 3.5 and 2.6 kg-polymer/g-cat./h, respectively, as shown in Figure 9(b).

The initial catalyst size exercises a significant influence on the number-average molecular weight. Indeed, Figure 10(a) shows that the molecular weight decreases from 230 to 170 and to 130 kg/mol as the catalyst size increases from 10 to 15 μ and to 20 μ , respectively. This is the result of the fact that the average monomer concentration in the polymer particle decreases as the size of initial catalyst increases. When the diffusional resistance is high because of the increased particle size, the average concentration of monomer in the macroparticle becomes low. Consequently, both the average rate of polymerization and the average molecular weight over the entire polymer particle would decrease as may be observed from Figures 9(b) and 10(a).

Figure 10(b) presents the variation of polydispersity for different initial catalyst sizes. The polydispersity turns out to be larger for the polymer produced by initially larger catalyst than by the smaller one. For a larger polymer particle the intraparticle gradient of monomer concentration would be fairly large because of the large diffusional resistance. This will bring about a significant variation of the polymer chain length in the

radial direction. Such a variation is believed to be the main cause for the large value of polydispersity, although the existence of two different kinds of active sites may also contribute to some extent.

CONCLUSIONS

A three-level hierarchical model is developed for a semibatch slurry reactor for olefin polymerization. The model assumes that the catalyst has two different kinds of active sites, and the quantity of cocatalyst is sufficient enough for all the potential sites to become active. Hydrogen gas is the only component involved in the chain transfer reaction. The multigrain model is used to describe the growth of the polymer particle from the original catalyst.

From the results of model simulation the hydrogen concentration is found to have practically no influence on the intraparticle diffusion of monomer, the microparticle growth factor, the size of macroparticle, and the polymer productivity. The steady-state value of polydispersity is independent of the hydrogen concentration when the hydrogen concentration is larger than a critical value. On the other hand, the number-average molecular weight is strongly dependent upon the hydrogen concentration. In particular, the number-average molecular weight turns out to be inversely proportional to the n th power of the hydrogen concentration, where n varies from 1/2 to 1 as the hydrogen concentration increases.

In contrast to the case of hydrogen concentration, the initial size of catalyst exercises a significant influence upon the voidage, the effectiveness factor, the macroparticle radius and the productivity. Consequently, the number-average molecular weight and the polydispersity are strongly dependent on the initial size of catalyst. On the basis of the above results, one may conclude that the large diffusional resistance in polymer particles caused by the initially large catalyst brings about a large value of polydispersity, although the presence of two different kinds of active sites may also contribute to some extent.

NOMENCLATURE

A	cocatalyst [mol/cat]
α_{gl}	gas-liquid interfacial area per unit volume of liquid and gas bubbles [m^2/m^3]

α_{ls}	liquid–solid interfacial area per unit volume of solid and liquid [m^2/m^3]	q_{exit}	rate of monomer leaving the reactor [mol/s]
cat	mass of catalyst [kg]	q_{in}	rate of monomer bubbled into the reactor [mol/s]
$C^*(j)$	vacant active site type j or its concentration [$\text{mol}/\text{m}^3 \cdot \text{cat}$]	q_{out}	rate of monomer going out from the slurry to the continuous gas phase [mol/s]
$C^*_0(j)$	total concentration of site type j [$\text{mol}/\text{m}^3 \cdot \text{cat}$]	Rate $_p$	volumetric rate of polymerization in macroparticle at a certain radial position [$\text{mol}/\text{m}^3 \cdot \text{s}$]
$C_p(j)$	potential active site of type j or its concentration [$\text{mol}/\text{m}^3 \cdot \text{cat}$]	Rate $_s$	rate of polymerization in microparticle at a certain radial position [$\text{mol}/\text{cat} \cdot \text{s}$] or [$\text{kg-polymer}/\text{g-catalyst} \cdot \text{h}$]
D_p	effective diffusivity of monomer in the macroparticle [m^2/s]	R_{cat}	radius of initial catalyst [m]
D_s	diffusivity of monomer in the microparticle [m^2/s]	$R_n(j)$	live polymer of site type j with n units or its concentration [$\text{mol}/\text{m}^3 \cdot \text{cat}$]
H_2	hydrogen gas concentration in the reactor [mol/m^3]	R_p	radius of macroparticle [m]
$k_{fH}(j)$	reaction rate constant of chain transfer to hydrogen [$\text{m}^3/\text{mol} \cdot \text{s}$]	R_s	radius of microparticle [m]
k_{gl}	mass transfer coefficient at the gas–liquid interface [m/s]	r_{crys}	radius of catalyst crystallite [m]
$k_I(j)$	initiation rate constant of site type j [$\text{m}^3/\text{mol} \cdot \text{s}$]	t	reaction time [s]
k_{ls}	mass transfer coefficient at the liquid–solid interface [m/s]	V^*	volume of continuous gas phase [m^3]
$k_p(j)$	propagation rate constant of site type j [$\text{m}^3/\text{mol} \cdot \text{s}$]	V_g	volume of gas bubble phase in the reactor [m^3]
M	monomer or its concentration [mol/m^3]	V_l	volume of liquid phase in the reactor [m^3]
M_{crys}	concentration of monomer at the surface of catalyst fragment [mol/m^3]	ν_{pol}	volume fraction in the swollen amorphous polymer [–]
M_l	concentration of monomer in the liquid phase [mol/m^3]	X_n	degree of polymerization [–]
M_l^*	concentration of monomer at the gas–liquid interface in equilibrium with the gas bubble phase [mol/m^3]	Greek Letters	
M_p	concentration of monomer in the macroparticle [mol/m^3]	ϵ	voidage in the polymer particle [–]
$M_{p,s}$	concentration of monomer at the surface of macroparticle [mol/m^3]	η^*	partition coefficient [–]
M_s	concentration of monomer in the microparticle [mol/m^3]	$\mu_k^L(j)$	k th moment of the concentration of live polymer of site type j [$\text{mol}/\text{m}^3\text{-cat}$]
M_n	number-average molecular weight [kg/mol]	$\mu_k^D(j)$	k th moment of the concentration of dead polymer of site type j [$\text{mol}/\text{m}^3\text{-cat}$]
M_w	weight-average molecular weight [kg/mol]	τ_s	time constant for the microparticle [s]
MW	molecular weight of monomer [kg/mol]	ϕ	microparticle growth factor [–]
P_{max}	upper limit of pressure in the continuous gas phase [Pa]	REFERENCES	
$P_n(j)$	dead polymer produced from site type j with n units or its concentration [$\text{mol}/\text{m}^3 \cdot \text{cat}$]	1.	Clark, A.; Bailey, G. C. <i>J Catal</i> 1963, 2, 230.
P_t	pressure in the continuous gas phase [Pa]	2.	Natta, G. <i>J Polym Sci</i> 1959, 34, 21.
PD	polydispersity [–]	3.	Buls, V. W.; Higgins, T. L. <i>J Polym Sci Part A-1</i> 1970, 8, 1025.
R	universal gas constant [$\text{J}/\text{mol} \cdot \text{K}$]	4.	Schmeal, W. R.; Streat, L. R. <i>AIChE J</i> 1971, 17, 1188.
		5.	Ray, W. H. <i>Proceeding of MMI Congress 1981</i> ; Cambridge Univ. Press: New York, 1988, p. 563.
		6.	Kakugo, M.; Sadatoshi, H.; Yokoyama, M.; Kojima, K. <i>Macromolecules</i> 1989, 22, 547.

7. Yermakov, Yu. I.; Mikhalchenko, V. G.; Beskov, V. S.; Grabovskii, Yu. P.; Emirova, I. V. *Plast Massy* 1970, 9, 7.
8. Taylor, T. W.; Choi, K.Y.; Yuan, H. G.; Ray, W. H. *Proceedings of the 1981 MMI Symposium on Transitional Metal Catalyzed Polymerization*, Midland; Plenum: New York, 1983.
9. Nagel, E. D.; Kirillov, V. A.; Ray, W. H. *Ind Eng Chem Prod Res Dev* 1980, 19, 372.
10. Galvan, R.; Tirrell, M. *Comput Chem Eng* 1986, 10, 77.
11. Hoel, E. L.; Cozewith, C.; Byrne, G. D. *AIChE J* 1994, 40, 1669.
12. Laurence, R. L.; Chiovetta, M. G. *Polymer Reaction Engineering: Influence of Reaction Engineering on Polymer Properties*; Carl Hanser Verlag: New York, 1983.
13. Floyd, S.; Choi, K. Y.; Taylor, T. W.; Ray, W. H. *J Appl Polym Sci* 1986, 32, 2935.
14. Hutchinson, R. A.; Chen, C. M.; Ray, W. H. *J Appl Polym Sci* 1992, 44, 1389.
15. Xie, T.; McAuley, K. B.; Hsu, J. C. C.; Bacon, D. W. *AIChE J* 1995, 41, 1251.
16. Ray, W. H. *Transition Metal Catalyzed Polymerizations*; Quirk, R. P., Ed.; Cambridge University Press: New York, 1988.
17. Natta, G.; Danusso, F.; Sianesi, D. *Makromol Chem* 1959, 30, 238.
18. Zakharov, V. A.; Bukatov, G. D.; Yermakov, Y. I. *Adv Polym Sci* 1983, 51, 61.
19. Floyd, S.; Choi, K. Y.; Taylor, T. W.; Ray, W. H. *J Appl Polym Sci* 1986, 31, 2231.
20. Treybal, R. E. *Mass Transfer Operations*; McGraw-Hill International Edition: Singapore, 1980, 3rd ed.
21. Prausnitz, J. M.; Lichtenthaler, R. N.; de Azevedo, E. G. *Molecular Thermodynamics of Fluid-Phase Equilibria*; Prentice-Hall: Englewood Cliffs, NJ, 1986, 2nd ed.
22. Reid, R. C.; Prausnitz, J. M.; Poling, B. E. *The Properties of Gases and Liquids*; McGraw-Hill: New York, 1988, 4th ed.
23. Choi, K.-Y.; Ray, W. H. *JMS-Rev Macromol Chem Phys* 1985, 25, 1.
24. Skomorokhov, V. B.; Zakharov, V. A.; Kirillov, V. A. *Macromol Chem Phys* 1996, 197, 1615.
25. Hoffman, A. S.; Fries, B. A.; Condict, P. C. *J Polym Sci* 1963, C4, 109.
26. Grievson, B. M. *Makromol Chem* 1965, 84, 93.
27. Kaminsky, W.; Luker, H. *Makromol Chem Rapid Commun* 1959, 5, 225.
28. Dutchke, J.; Kaminsky, W.; Luker, H. *Polymer Reaction Engineering*; Hanser Publishers: Munich, 1983, p. 209.
29. Doi, Y.; Ueki, S.; Keii, T. *Makromol Chem* 1979, 180, 1359.
30. Böhm, L. L. *Polymer* 1978, 19, 562.
31. Young, R. J.; Lovell, P. A. *Introduction to Polymers*; Chapman & Hall: London, 1991, 2nd ed.
32. Reich, L.; Schindler, A. *Polym Rev* 1966, 12, 326.
33. Berger, M. N.; Boocock, G.; Haward, R. N. *Adv Catal* 1969, 19, 24.
34. Taylor, W. C.; Tung, L. H. *Polym Lett* 1963, 1, 157.
35. Keii, T. Paper at the MMI Int Symp on Transition Metal Catalyzed Polymerization: Unsolved Problems, Midland, August 1981.
36. Yuan, G. G.; Taylor, T. W.; Choi, K. Y.; Ray, W. H. *J Appl Polym Sci* 1982, 27, 1691.
37. Pegoraro, M. *Chim Ind (Milan)* 1962, 44, 18.
38. Chien, J. C. W.; Wang, B.-P. *J Polym Sci Part-A Polym Chem* 1990, 28, 15.
39. Ivanchev, S. S.; Baulin, A. A.; Rodionov, A. G. *J Polym Sci Polym Chem Ed* 1980, 18, 2045.